

Fig.S1. Analysis of heart outflow tract phenotype in *Lrp2*^{-/-} mutants and controls.

C57BL/6N and FVB/N control hearts (refers to *Lrp2*^{+/+} and *Lrp2*^{-/-} samples) at E18.5 by stereomicroscopic inspection (**A, G**) and polymeric dye injection (**B, H**).

In controls, injection of Batson's red polymeric dye into the left ventricle (LV) after cutting the ductus arteriosus indicated the ascending aorta in red (AA). Injection of blue polymeric dye into the right ventricle (RV) labeled the pulmonary artery in blue (PA). Frontal plane H&E-stained paraffin sections through hearts of control embryos (**E, E'**, **K, K'**) depicted normally separated ascending aorta (AA) and pulmonary artery (PA). *Lrp2*^{-/-} mutants (15/16) on C57BL/6N background suffered from common arterial trunk (CAT), (**C**, arrowhead). 1/16 mutant suffered from double outlet right ventricle (DORV, see **Table S1**). Injection of the red polymeric dye into the mutant's left ventricle followed by injection of blue ink into the right ventricle showed both dyes in the CAT and indicated an additional ventricular septum defect (**D**, arrowhead). CAT in *Lrp2*^{-/-} C57BL/6N embryos was also shown on H&E-stained frontal heart sections (**F, F'**). No CAT was detected in *Lrp2*^{-/-} mutants on FVB/N background (n = 13, **I, J, L, L'**). 85% of *Lrp2*^{-/-} FVB/N embryos displayed a normal heart morphology with a proper connection of the ascending aorta to the left ventricle and of the pulmonary artery to the right ventricle. 2 out of 13 *Lrp2*^{-/-} FVB/N mice showed DORV (**Table S1**). Scale bars: 1 mm.

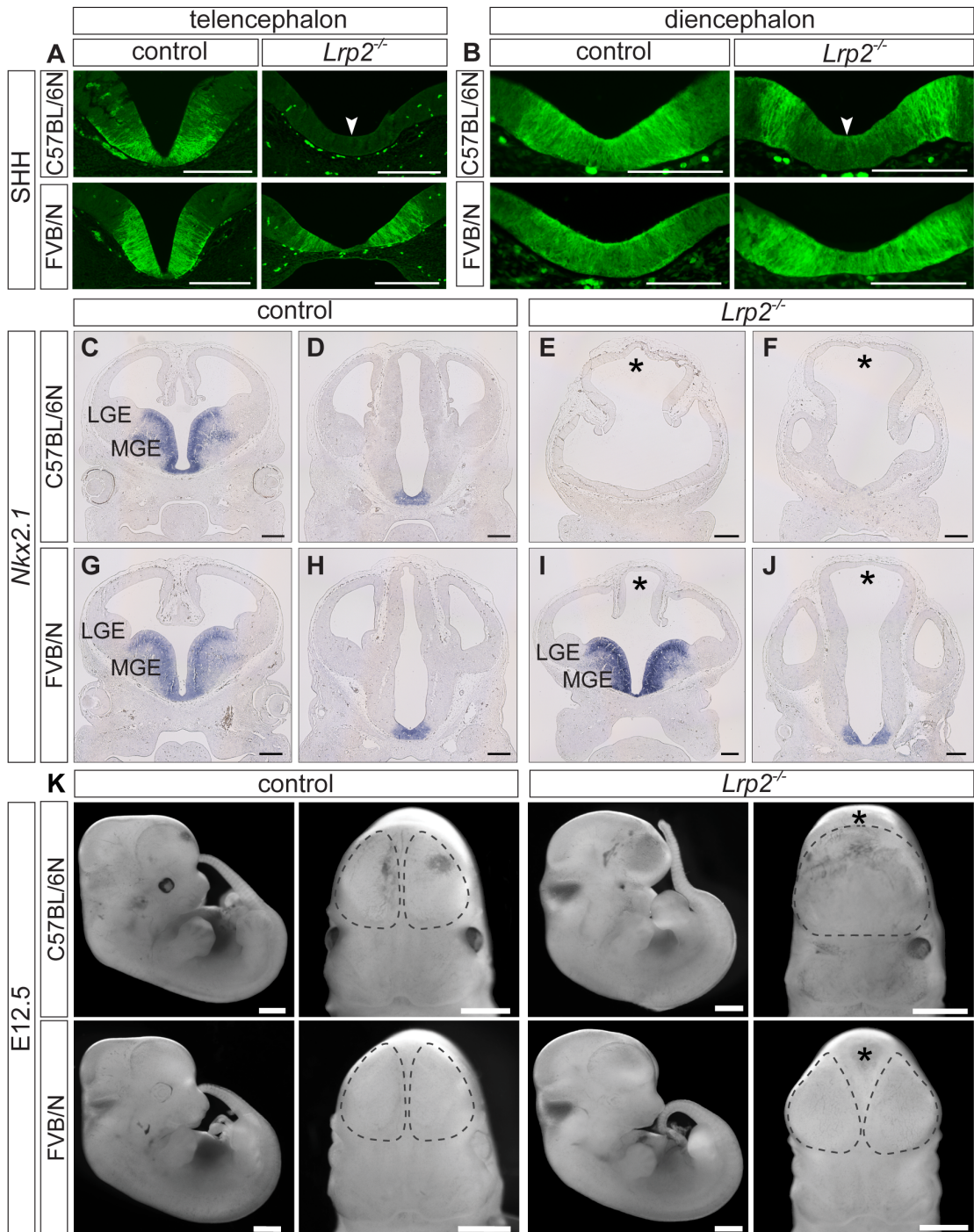


Fig. S2. Loss of ventral forebrain SHH and *Nkx2.1* in *Lrp2*^{-/-} C57BL/6N mice, leading to HPE, is rescued in mutants on a FVB/N background. Related to Fig. 2.

(A - B) Immunohistological detection of SHH (green) on coronal sections of the forebrain in control (refers to *Lrp2*^{+/+} and *Lrp2*^{+/-}) and somite matched *Lrp2*^{-/-} embryos at E10.5.

(A) SHH protein was lost in the ventral telencephalon of *Lrp2*^{-/-} C57BL/6N embryos (arrowhead), (n = 3) compared with controls (n = 5). *Lrp2*^{-/-} mice on a FVB/N background displayed normal SHH protein localization in the ventral telencephalon (n = 6), comparable to controls (n = 7). Scale bars: 250 μ m.

(B) SHH signal in the ventral midline of the diencephalon (arrowhead) was decreased and shifted to more lateral domains in *Lrp2*^{-/-} C57BL/6N embryos (n = 3) compared with controls (n = 5). *Lrp2*^{-/-} FVB/N embryos presented with a normal SHH pattern (n = 6), similar to controls (n = 7). Scale bars: 100 μ m.

(C - J) In situ hybridization (ISH) for *Nkx2.1* on coronal forebrain paraffin sections from embryos at E12.5.

The medial ganglionic eminence (MGE) and the lateral ganglionic eminence (LGE) were formed in controls. The MGE was positive for *Nkx2.1* signals in controls (**C**, **G**). *Nkx2.1* signals were also detected in the ventral midline of the diencephalon (**D**, **H**). In *Lrp2*^{-/-} C57BL/6N embryos (n = 3), *Nkx2.1* expression was lost in the MGE region, which is hypoplastic in the mutants (**E**), and there was no *Nkx2.1* signal in the ventral diencephalon (**F**) compared with controls (n = 3). In contrast, all *Lrp2*^{-/-} FVB/N embryos (n = 3) displayed a normal expression pattern for *Nkx2.1* (**I**, **J**) comparable to controls (n = 2). Note the dilation of the dorsal forebrain midline in *Lrp2* null mutants on both strains (**E**, **F**, **I**, **J**, asterisks). Scale bars: 250 μ m.

(K) Phenotypic characterization of control embryos and *Lrp2*^{-/-} mutants on a C57BL/6N and a FVB/N background at E12.5, presented in a lateral view and of embryonic heads presented in a frontal view. 100% of *Lrp2*^{-/-} C57BL/6N embryos (n = 21) displayed severe forebrain malformations, small eyes and a single forebrain hemisphere (dashed line circle) compared with controls (n = 31). 100% of *Lrp2*^{-/-} FVB/N embryos (n = 52) showed normal HPE appearance in the lateral view comparable to controls (n = 102). They developed separated forebrain hemispheres (dashed line circles), highlighted in the frontal view. A dilation of the dorsal diencephalon was however visible in the frontal view of the LRP2-deficient FVB/N embryos (asterisk) as well as in the *Lrp2*^{-/-} C57BL/6N embryos (asterisk). Scale bars: 1 mm.

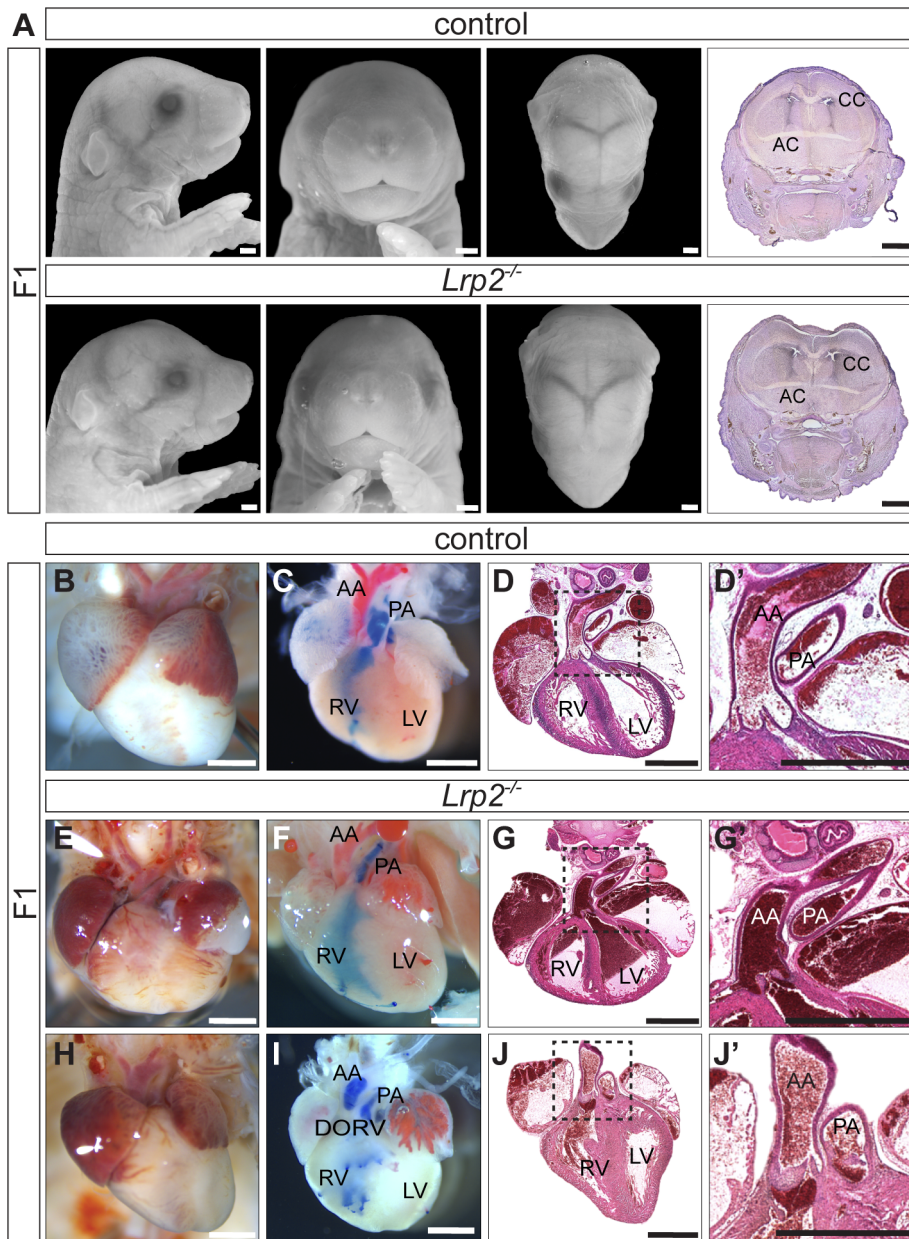


Fig. S3. Rescue of congenital defects in *Lrp2*^{-/-} mutants on a hybrid F1 (C57BL/6N; FVB/N) background. Related to Fig. 3.

(A) E18.5 embryonic heads shown in the sagittal, frontal and dorsal views. All *Lrp2*^{-/-} F1 mutants (n = 59) showed normal craniofacial features compared with controls (*Lrp2*^{+/+} and *Lrp2*^{+/-}; n = 91). NISSL stained coronal cryosections of E18.5 *Lrp2*^{-/-} heads on a F1 background (n = 17) showed normally separated ventricles, normal corpus callosum (CC) as well as anterior commissure (AC) structures comparable to controls (n = 16). Scale bars: 1 mm.

(B - J) Analysis of heart phenotype in E 18.5 embryos.

Stereomicroscopy images of hearts from control F1 embryos (B; n= 15) and from *Lrp2*^{-/-} F1 embryos (E, H; n = 27).

Batson's red polymeric dye injection into the left ventricle, followed by injection of blue polymeric dye into the right ventricle in control F1 embryos (C; n= 3) and in *Lrp2*^{-/-} F1 embryos (F, I; n = 4).

Frontal plane of H&E-stained paraffin sections through hearts of control embryos (D, D'; n = 6) and *Lrp2*^{-/-} F1 embryos (G, G', J, J'; n = 5) demonstrated the outflow tract anatomy.

55.6% (5/9) of *Lrp2*^{-/-} F1 embryos showed normal heart morphology and outflow tract anatomy (E - G) compared with controls (B - D). 44.4% *Lrp2*^{-/-} F1 mice (4/9) showed a double outlet right ventricle (DORV) (H - J). Importantly, a common arterial trunk (CAT) phenotype was never observed in any of the *Lrp2* F1 mutants

(0/27). This suggests a partial rescue of the heart outflow defects in *Lrp2* F1 mutants compared with *Lrp2*^{-/-} mutants on a C57BL/6N background (see Fig. S1 and Table S1). Scale bars: 1 mm. AA: ascending aorta; PA: pulmonary artery; LV: left ventricle; RV: right ventricle.

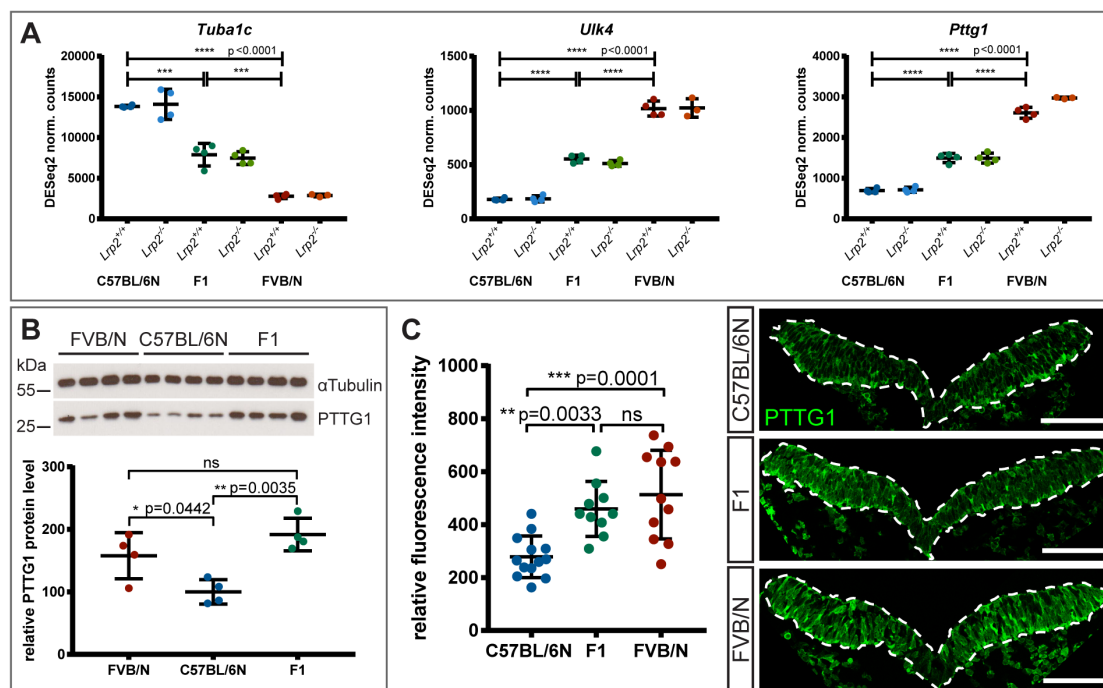


Fig. S4. Candidate modifier gene expression and PTTG1 localization in cell culture and *in vivo*. Related to Fig. 4.

(A) DESeq2 normalized counts for *Tuba1c*, *Ulk4* and *Pttg1*. *Tuba1c* showed significantly lower expression levels for F1 and FVB/N backgrounds compared with C57BL/6N. *Ulk4* and *Pttg1* showed significantly higher expression levels in embryonic head samples of both genotypes on a FVB/N and F1 compared with C57BL/6N background. Data are mean \pm s.d.

(B) Western blot analysis of total PTTG1 protein levels in FVB/N, C57BL/6N, and F1 E8.5 *Lrp2*^{+/+} embryos (13 somites; n = 4 for each background). PTTG1 signals, normalized to α -tubulin, showed significantly higher PTTG1 levels in FVB/N and F1 compared with C57BL/6N embryos. Scatter plot presents mean \pm s.d.; significance was assessed with one-way ANOVA; * p < 0.05, ns: not significant.

(C) Immunofluorescence intensity of PTTG1 protein (green) was measured in the neuroepithelium (dashed line) from E8.5 C57BL/6N (n = 5), F1 (n = 3) and FVB/N (n = 4) control embryos (*Lrp2*^{+/+} and *Lrp2*^{+/-}). A total of 3 coronal sections from each embryo (10 and 11 somites) were examined. Significantly higher PTTG1 protein levels were found in the FVB/N and F1 embryos compared with C57BL/6N. Scatter plot presents mean \pm s.d.; the significance was assessed with one-way ANOVA; ** p < 0.01, *** p < 0.001. Scale bars: 100 μ m.

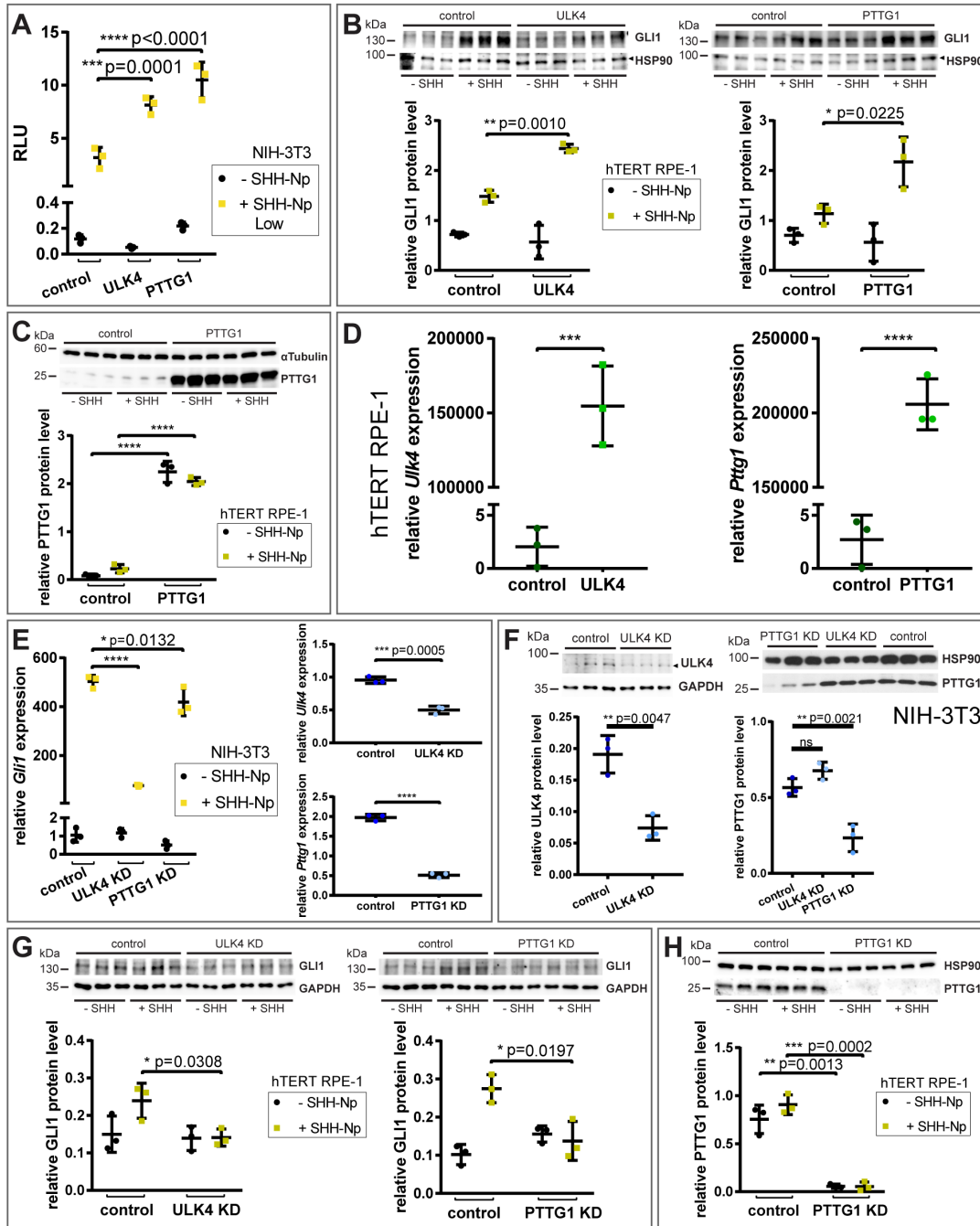


Fig. S5. Analyses of SHH stimulated pathway response in gain- and loss-of-function assays for ULK4 and PTTG1 *in vitro*. Related to Fig. 5.

(A) SHH responsive GLI-Luciferase reporter assay on NIH-3T3 cells with 1:20 diluted SHH conditioned medium (SHH-Np low). Significant increase of relative GLI-driven luciferase levels was observed for *Ulk4* and *Pttg1* overexpression, respectively compared with the control after SHH stimulation. Note higher fold changes in context of lower SHH stimulation – 2.6 fold and 3.3 fold changes for ULK4 and PTTG1, respectively (compared to 1.4 and 1.5 fold changes, respectively in Fig. 5A). Significance assessed with two-way ANOVA; **** $p < 0.0001$; RLU: relative light units. Data are mean \pm s.d.

(B) Western blot analysis of endogenous GLI1 protein levels after *Ulk4* and *Pttg1* overexpression in hTERT RPE-1 cells. Significant induction of GLI1 levels was observed after overexpression of *Ulk4* and *Pttg1*, respectively. Significance was assessed with two-way ANOVA; * $p < 0.05$. Data are mean \pm s.d. The overexpression of *Ulk4* and *Pttg1* was validated by Western blot **(C)** and by qRT-PCR **(D)**; unpaired t-test; **** $p < 0.0001$.

(E) Relative *Gli1* mRNA expression level analysis by qRT-PCR in NIH-3T3 cells showed that ULK4 and PTTG1 knockdown (KD) significantly compromised the increase in *Gli1* mRNA levels after SHH stimulation compared with controls. Significance assessed by two-way ANOVA; **** $p < 0.0001$. The ULK4 and PTTG1 KD was validated by qRT-PCR for *Ulk4* and *Pttg1* expression, respectively **(E)** and by Western blot **(F)**; unpaired t-test; **** $p < 0.0001$. Data are mean \pm s.d.

(G) Western blot analysis of endogenous GLI1 protein levels after ULK4 and PTTG1 KD, respectively in hTERT RPE-1 cells demonstrated significantly lower GLI1 levels after SHH stimulation compared with controls. The PTTG1 KD was validated by Western blot **(H)**; unpaired t-test; * $p < 0.05$. Data are mean \pm s.d.

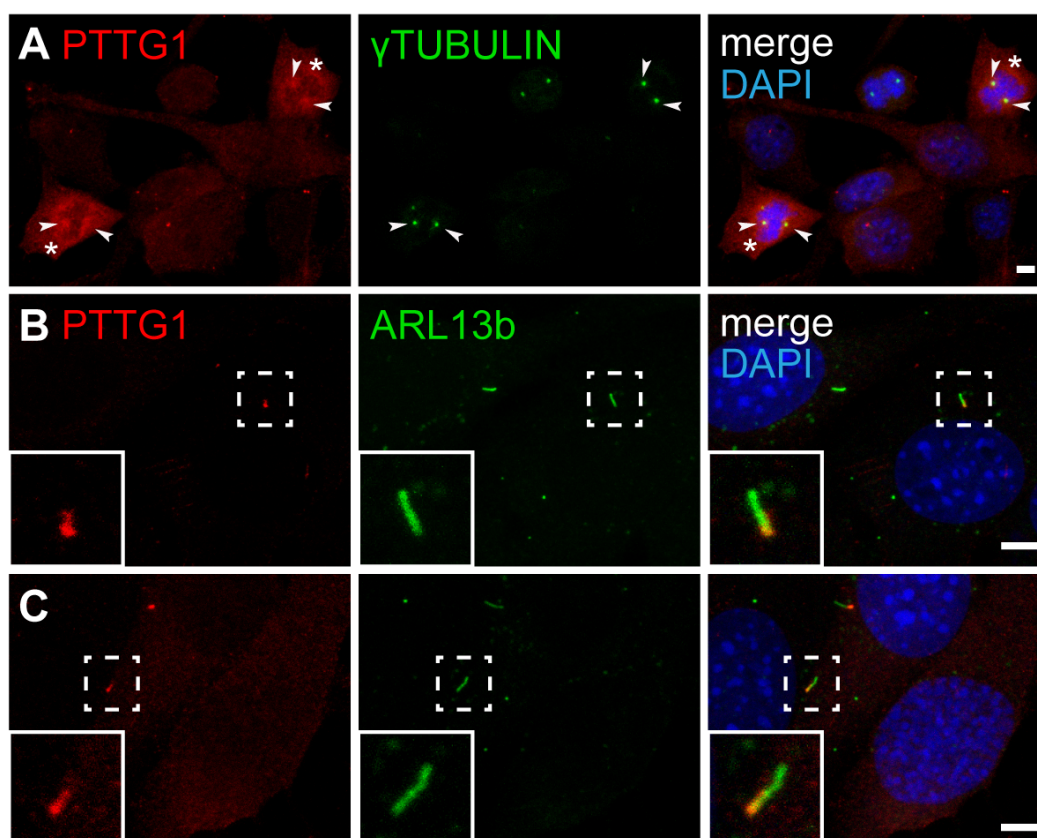


Fig. S6. Subcellular localization of PTTG1 in NIH-3T3 cells by immunofluorescence confocal microscopy. Related to Fig. 6.

PTTG1 immunostaining (red) was detected in mitotic NIH-3T3 cells at the perinuclear region, concentrated at the centrosomes (**A**, arrowheads) positive for γ -tubulin (green) and in the cytoplasm (**A**, asterisks). Quiescent/interphase cells (**B**, **C**) showed PTTG1 localization in primary cilia, immunolabeled for ARL13b (green). PTTG1 signals were detected at the base (**B**), as well as along the ciliary shaft (**C**). Insets show the magnification of the chosen cilia (dashed line squares). Experiments were repeated at least five times in triplicates. DAPI (blue) marks nuclei. Scale bars: 5 μ m.

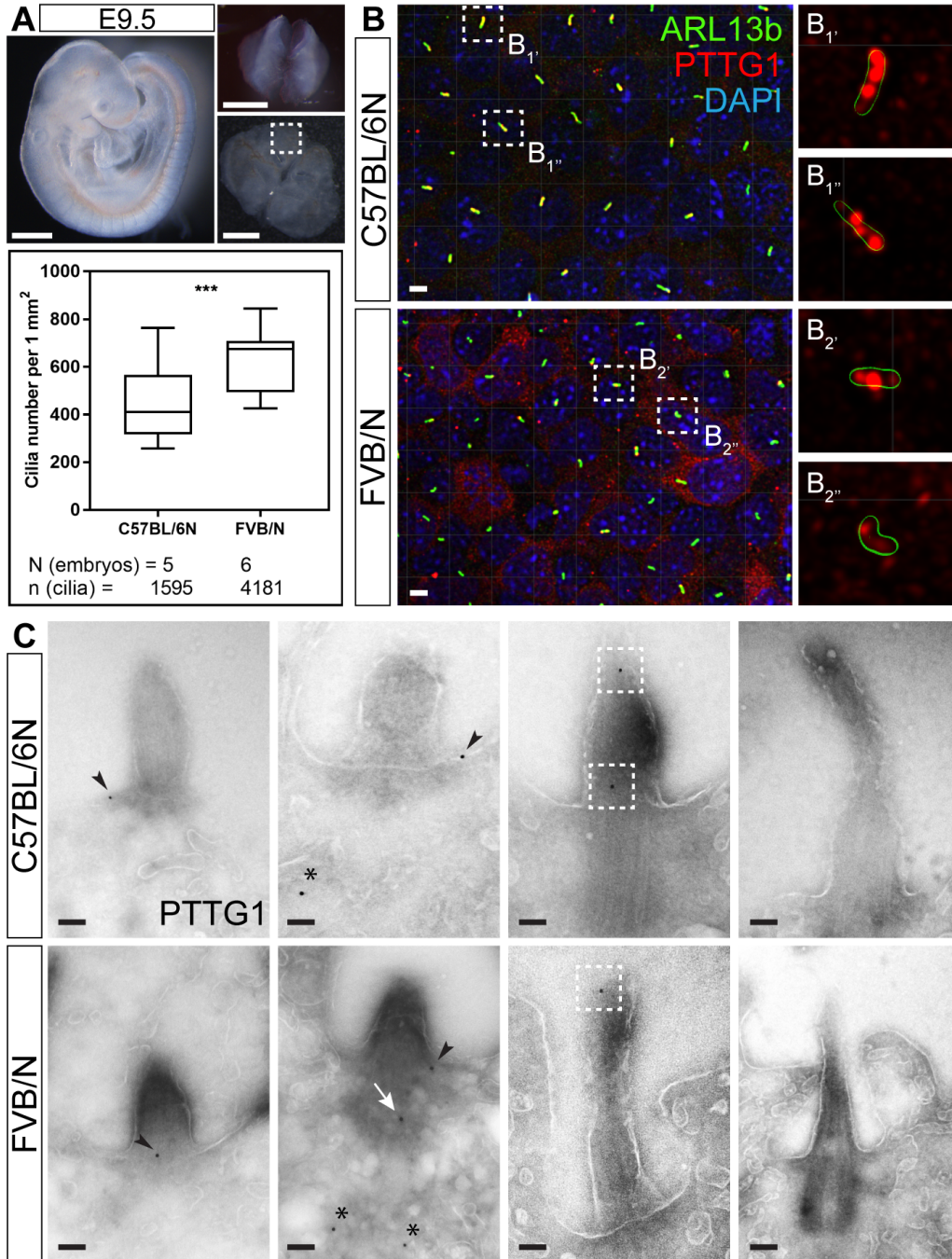


Fig. S7. Analysis of primary cilia and ciliary PTTG1 localization. Related to Fig. 7.

(A) E9.5 embryos were used to prepare cephalic explants in order to examine the primary cilia of the mouse neuroepithelium. Images show the side view on the E9.5 embryo, head after opening the neural tube and flattened explants ready for the immunofluorescence staining. Dashed line square indicates the forebrain region of interest. Scale bars: 500 μm .

(B) Confocal microscopy images of the en face view on the neuroepithelium from *Lrp2*^{+/+} C57BL/6N and FVB/N embryos showed two aspects: 1) PTTG1 localization to a subset of cilia, immunolabeled for ARL13b (green), in both strains; 2) differences in the cilia number per neural tube area between the two strains. Two representative primary cilia for each strain are shown in higher magnification (**B**₁, **B**₁'', **B**₂, **B**₂'') and display PTTG1 localization to the ciliary shaft for both backgrounds. Green reconstructed ARL13b staining show the circumference of each cilium. Scale bars: 1 μm .

The box plot represents the quantification of the average cilia number per 1 mm² area with whiskers indicating minimal and maximal values. N = 5 C57BL/6N and N = 6 FVB/N embryos were analyzed and a total cilia number of n = 1595 and n = 4181, respectively, was quantified. Unpaired t-test statistical analysis was performed; *** p < 0.001.

(C) Immunogold labeling of PTTG1 in the primary cilium of E9.5 C57BL/6N and FVB/N neuroepithelium. PTTG1 localized to a subset of primary cilia and was found in periciliary region (arrowheads), the basal body (arrow), the ciliary shaft (boxed), and in the cytoplasm (asterisks), confirming the observations from the confocal microscopy. Representative images for C57BL/6N and FVB/N show cilia positive for PTTG1 (three left panels) and one cilium without PTTG1 signals (right panel). 2 embryos for each strain were analyzed for immunogold labeling; experiments were repeated 5 times with a number of 40 sections analyzed for each experiment. Scale bars: 100 nm.

Table S1. Frequency of congenital heart defects in *Lrp2*^{-/-} embryos and controls on different strain backgrounds. Related to Fig. S1 and S3

The table indicates the number of embryos analyzed for each genotype by polymeric dye injection into the heart and by heart histology and the numbers on phenotype penetrance.

CAT: common arterial trunk; DORV: double outlet right ventricle

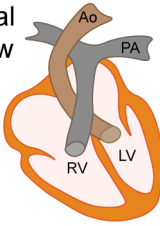
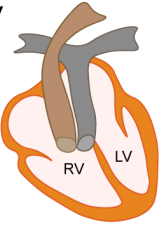
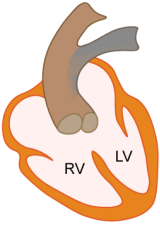
	 Normal outflow tract	 DORV	 CAT
C57BL/6N control	7	0	0
C57BL/6N <i>Lrp2</i> ^{-/-}	0	1	15
FVB/N control	11	0	0
FVB/N <i>Lrp2</i> ^{-/-}	11	2	0
F1 control	9	0	0
F1 <i>Lrp2</i> ^{-/-}	5	4	0

Table S2. List of differentially expressed genes (DEGs) from all comparisons

[Click here to download Table S2](#)

Table S3. Unfiltered and filtered lists of DEGs from strain-specific comparisons

[Click here to download Table S3](#)